Hindawi
Advances in Condensed Matter Physics
Volume 2024, Article ID 5630225, 11 pages
https://doi.org/10.1155/2024/5630225

Research Article

Unlocking the Magnetic and Half-Metallic Properties of AMY_2 (A = Cu, Ag; M = Sc, Ti, V, Cr, Mn, Fe; Y = S, Se) Compounds in Chalcopyrite Structure: An *Ab Initio* Study for Spintronics Applications

D. Vijayalakshmi,[1,2] **Tholkappiyan Ramachandran**,[3,4] **G. Jaiganesh**,[5] **G. Kalpana**,[1] **and Fathalla Hamed**[6]

[1]*Department of Physics, College of Engineering, Anna University, Chennai 600 025, India*
[2]*Department of Physics, Vels Institute of Science, Technology and Advanced Studies (VISTAS) Pallavaram, Chennai 600117, Tamil Nadu, India*
[3]*Department of Physics, Saveetha School of Engineering, Saveetha Institute of Medical and Technical Science, Saveetha University, Chennai 602105, India*
[4]*Department of Physics, Khalifa University of Science and Technology, Abu Dhabi P. O. Box 127788, UAE*
[5]*Excel Instruments, Gala, No. 9/10 Building No. 2 Dias Industrial Estate, East Sativali Naka – 401208, Vasai, India*
[6]*Department of Physics, College of Science, United Arab Emirates University, Al-Ain P.O.X. 15551, UAE*

Correspondence should be addressed to G. Kalpana; g_kalpa@annauniv.edu

Received 9 November 2023; Revised 28 March 2024; Accepted 23 April 2024; Published 20 May 2024

Academic Editor: Sefer Bora Lisesivdin

We present an investigation into the magnetism exhibited by AMY_2 compounds characterized by a chalcopyrite structure, where A can be Cu or Ag, M can be Sc, Ti, V, Cr, Mn, or Fe, and Y can be either S or Se. By substituting M atoms at the Ga position of $AGaY_2$ compounds, the magnetic properties were calculated using the full potential linearized augmented plane wave method under the generalized gradient approximation and local spin density approximation with the WIEN2K code. The obtained spin-polarized results confirmed the presence of ferromagnetic and half-metallic (HM) properties in AMY_2 compounds (A = Cu, Ag; M = Ti, V, Cr, Mn; Y = S, Se), wherein the HM property is preserved through p-d hybridization of p states of Y (S, Se) atoms with d (t_{2g}) states of M (M = Ti, V, Cr, Mn) atoms, and minimal contribution of −s states of A (A = Cu, Ag) atoms. The total magnetic moments for AMY_2 compounds were calculated as 1.00, 2.00, 3.00, and 4.00 μ_B/f.u. for M = Ti, V, Cr, Mn, respectively. For $AFeY_2$ compounds (A = Cu, Ag; Y = S, Se), electronic band structures for both up spin and down spin states were identical, suggesting antiferromagnetic behavior at equilibrium, while $AScY_2$ compounds (A = Cu, Ag; Y = S, Se) exhibited nonmagnetic properties at equilibrium. Overall, the accurate HM properties of AMY_2 materials suggest promising prospects for their utilization in spintronics and magnetic storage device applications.

1. Introduction

Materials possessing half-metallic ferromagnetic (HMF) properties have garnered substantial interest in the realm of spintronic applications [1–4]. Initially, the focus was on transition metal (TM) doped binary systems like InAs, GaAs, ZnO, and GaN [5–8], owing to their predicted high Curie temperature ($T_C \geq 300$ K). As a result, research on TM-doped binary semiconductors has received significant attention in both theoretical and experimental aspects of spintronics [9–11]. However, despite exhibiting ferromagnetism (FM), binary FM semiconductors encounter challenges in practical spintronic applications due to the rapid loss of spin polarization through spin-flip scattering, attributed to the low solubility of magnetic ions in the binary substrates [4, 5, 12, 13]. To address these limitations, the search for new HMF materials

with compatibility with traditional semiconductors' structure and lattice matching has become imperative, opening possibilities for practical applications in spintronics when coated as thin films [14].

I–III–VI_2 type chalcopyrite compounds are ternary analogs of II–VI type zinc blende (ZB) structured compounds, characterized by the tetragonal-chalcopyrite structure with the tetrahedral space group I-42d and four formula units per unit cell [6–8, 14, 15]. These materials have found wide application in various technological domains, such as dielectrics, mid-infrared sources, photovoltaic applications [16, 17], and spintronics [18], due to their wide energy bandgap and low melting point. Notably, research intensity has increased due to the possibility of substituting TM atoms at one of the two cation sites, overcoming spin-flip scattering, and maintaining an asymmetrical crystal structure by exploiting the low solubility of magnetic ions in nonmagnetic semiconducting hosts [19].

Several reports have highlighted the FM observation in I–III–VI_2 type chalcopyrite compounds, including $CuAlS_2$, $CuInSe_2$, $CuGaSe_2$, $CuInS_2$, $CuFeS_2$, and $AgGaY_2$ (Y = S, Se), upon substituting TM (V, Cr, Mn, and Fe) atoms at group III sites, making them promising materials for spintronics applications [19]. Experimental studies have confirmed FM ordering in Mn-doped $ZnSnAs_2$ [20], $ZnGeP_2$, $CdGeP_2$ [21], Zn(GeSn)As_2, bulk $MnGeP_2$, and $MnGeAs_2$ [22]. Additionally, the possibility of antiferromagnetic (AFM) in Mn-doped II-Ge-V_2 (II = Cd, Zn; V = P, As) at $T = 0$ K has been reported [23]. Notably, the substitution site plays a crucial role in achieving carrier-mediated FM, as demonstrated when Mn is substituted on the Ge site of II-Ge-V_2, leading to the generation of holes and stabilization of FM [23]. Similarly, the substitution of Mn at group III sites in $CuInSe_2$, $CuInS_2$, $CuAlS_2$, and $CuInTe_2$ chalcopyrite compounds has been observed to produce holes, signifying FM stabilization [16]. An interesting AFM property has also been observed when Mn is substituted at the Cu site [16]. However, the underlying origins of these unique FM and AFM properties remain unclear, necessitating further experimental investigations [24].

Driven by these discoveries, the current study is driven by a desire to develop deeper insight into the intricate electronic configurations and magnetic properties exhibited by AMY_2 compounds (with A representing Cu or Ag, M representing Sc, Ti, V, Cr, Mn, or Fe, and Y representing S or Se) within the structured framework of chalcopyrite. Employing sophisticated first-principles methodologies facilitated by the WIEN2k code, we have utilized exchange-correlation functionals incorporating generalized gradient approximation (GGA) [21] and local spin density approximations (LSDA) [22].

It is worth noting that there is a notable scarcity of theoretical computations and experimental observations for $AgMY_2$ compounds, thus making this investigation the pioneering endeavor to conduct band structure calculations for these materials, particularly in the context of their potential applications in spintronics. The manifestation of HMF within $AgMY_2$ compounds, where M encompasses Ti, V, Cr, or Mn and Y represents S or Se, presents an exciting avenue for driving advancements in spin-based device technologies. This realization holds significant promise for the development of innovative applications harnessing the unique properties of these materials.

2. Crystal Structure and Methodology

$AGaY_2$ (A = Cu, Ag; Y = S, Se) compounds crystallize in the chalcopyrite structure [4, 25, 26] with the space group I−42d, and their atomic positions can be described as A1 (0, 0, 0), A2 (0, 1/2, 1/2); Ga_1 (1/2, 1/2, 0); Ga_2 (1/2, 0, 1/4), Y1 (u, 1/4, 1/8); Y2 (u, 3/4, 1/8); Y3 (3/4, u, 7/8); Y4 (1/4, u, 7/8), comprising two molecules per unit cell. The internal parameter u determines the anion displacement and results in two unequal anion–cation bond lengths, with the anions being closer to one pair of cations than the other. Each Y (S/Se) anion is coordinated with two Cu/Ag and two M/Ga cations in the chalcopyrite structure. The unit cell experiences tetragonal distortion, characterized by the internal parameter u, with $\eta = c/2a \approx 1$. AMY_2 compounds are derived by substituting Ga atoms with TM ions (M = Sc, Ti, V, Cr, Mn, Fe) in $AGaY_2$ (A = Cu, Ag; Y = S, Se) while preserving the chalcopyrite structure with nearly equal $c/2a$ ratio.

The calculations were performed using the full potential linearized augmented plane wave (FP-LAPW) method based on spin-polarized density functional theory (DFT) within LSDA and GGA, as implemented in the WIEN2k code [23, 24]. This method involves expanding the electronic wave function, crystal potential, and charge density into two basis sets. Wave functions are expanded in spherical harmonics within each atomic sphere region, while a plane wave basis set is used in the interstitial region. The crystal potential within the muffin-tin sphere is assumed to be spherically symmetric and constant in the interstitial region. Valence wave functions inside the sphere are expanded up to $l_{max} = 10$, and a plane wave Fourier series is employed with a cutoff of $k_{max} = 7.0/\text{RMT}$ in the interstitial region, with RMT being the muffin-tin radius. The charge density is Fourier expanded up to $G_{max} = 12$. The specific values of RMT for each element are considered 2.08, 2.12, 2.18, 2.23, 2.24, 2.16, 2.14, 2.02, 2.05, and 2.09 for Ag, S, Se, Sc, Ti, V, Cr, Mn, and Fe, respectively, in $AgMY_2$ compounds. For $CuMY_2$ compounds, the RMT values are set as 2.2, 2.3, 2.1, 2.4, 2.3, 2.1, 2.2, 2.3, and 2.4 for Cu, Sc, Ti, V, Cr, Mn, Fe, S, and Se, respectively. The integration of k-points is carried out using a $15 \times 15 \times 7$k mesh in the irreducible wedge of the Brillouin zone for both $CuGaY_2$ and $AgGaY_2$ compounds.

3. Results and Discussion

Atomic and equilibrium lattice positions play a crucial role in determining the magnetic and electronic properties of solids. Therefore, before conducting calculations for electronic and magnetic properties, we first perform full atomic position and volume optimization for two host materials, $AGaY_2$ (A = Cu, Ag; Y = S, Se) and AMY_2 (A = Cu, Ag; M = Sc, Ti, V, Cr, Mn, Fe; Y = S, Se), using the GGA and LSDA methods for NM, FM, and AFM states [27, 28]. It is worth noting that the calculated results for $AgMY_2$ and $CuMY_2$ are identical under both GGA and LSDA. Hence, the volume optimization

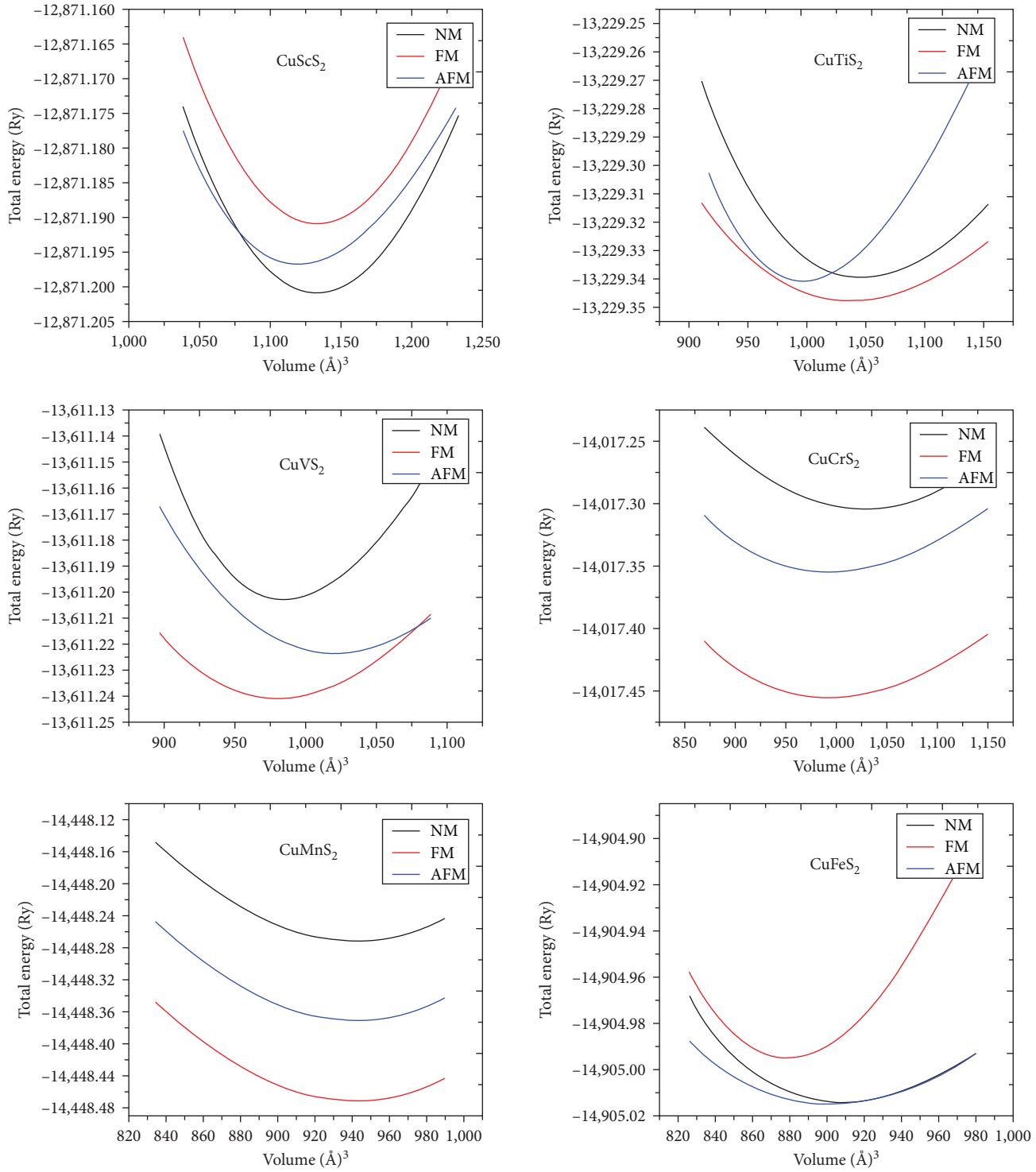

FIGURE 1: Total energy (Ry)/f.u. as a function of volume ($Å^3$) plots for nonmagnetic (NM), ferromagnetic (FM), antiferromagnetic (AFM) phases of $CuMS_2$ (M = Sc, Ti, V, Cr, Mn, Fe) compounds using GGA.

(energy–volume) curve for $CuMY_2$ compounds under GGA is presented in Figure 1.

From Figure 1, it is observed that the introduction of M (Sc, Ti, V, Cr, Mn, Fe) atoms into the NM host $AGaY_2$ (A = Cu, Ag; Y = S, Se) transforms them into FM or AFM materials. Specifically, for $CuMS_2$ (M = Ti, V, Cr, Mn), the FM state exhibits the minimum energy compared to the NM and AFM states. On the other hand, for $CuFeS_2$, the AFM phase demonstrates the lowest energy compared to the NM and FM phases, suggesting its stability in the AFM state at equilibrium. In contrast, for $CuScY_2$ compounds, the NM phase has the lowest energy, indicating that these compounds are stable in the NM state at equilibrium (Figure 1). Similar findings were obtained for $AgScY_2$ compounds also.

Table 1: Calculated internal parameter (u), equilibrium lattice constants (a_0, c_0) in Å, and bulk modulus (B_0) in GPa, total energy difference ΔE_1 ($\Delta E_1 = E_{FM} - E_{NM}$) in meV/cell, ΔE_2 ($\Delta E_2 = E_{FM} - E_{AFM}$) in meV/cell between the nonmagnetic (NM), ferromagnetic (FM), and antiferromagnetic (AFM) states of $CuMY_2$ (M = Sc, Ti, V, Cr, Mn, Fe; Y = S, Se) using GGA.

Compounds	NM				FM				AFM				ΔE_1	ΔE_2
	u	a_0	c_0	B_0	u	a_0	c_0	B_0	u	a_0	c_0	B_0		
$CuGaS_2$	0.248	5.35	10.76	74.8	0.248	5.36	10.74	74.4	0.248	5.34	10.79	75.2	—	—
Others	0.249[a]	5.37[a]	10.74[a]	75.1[a]	—	—	—	—	—	—	—	–	—	—
$CuScS_2$	0.232	5.82	10.01	72.24	0.230	5.804	9.97	72.22	0.228	5.81	9.95	72.22	−8.1	−5.6
$CuTiS_2$	0.244	5.45	10.63	80.38	0.242	5.43	10.63	80.36	0.240	5.41	10.53	80.36	−81.6	−56.9
$CuVS_2$	0.250	5.38	10.50	96.01	0.248	5.36	10.50	95.99	0.246	5.32	10.48	95.99	−1.7	−2.6
$CuCrS_2$	0.265	5.49	10.72	184.7	0.263	5.47	10.72	184.5	0.261	5.46	10.70	184.5	−14.7	−9.7
$CuMnS_2$	0.247	5.41	10.50	102.4	0.245	5.39 (5.39[b])	10.50 (10.57[b])	102.2	0.243	5.39	10.47	102.2	−73.4	−58.4
$CuFeS_2$	0.275	5.17	10.09	108.4	0.273	5.15	10.09	108.2	0.271	5.14	10.04	107.9	−2.01	0.223
$CuGaSe_2$	0.243	5.64	11.30	59.2	0.244	5.68	11.31	60.6	0.244	5.66	11.30	61.1	—	—
Others	0.244[a]	5.67[a]	11.34[a]	60.3[a]	—	—	—	—	—	—	—	—	—	—
$CuScSe_2$	0.245	5.61	11.17	63.56	0.241	5.63	11.14	63.53	0.242	5.69	11.16	63.56	—	—
$CuTiSe_2$	0.231	5.87	11.51	68.24	0.229	5.85	11.49	68.22	0.231	5.84	11.48	68.11	−19.3	−6.8
$CuVSe_2$	0.241	5.66	11.17	74.36	0.239	5.68	11.15	74.36	0.237	5.68	11.13	74.32	−12.1	−31.2
$CuCrSe_2$	0.249	5.64	11.10	67.14	0.247 (0.249[c])	5.64 (5.60[c])	11.07 (11.28[c])	67.14	0.245	5.64	11.07	67.08	−72.8	−65.3
$CuMnSe_2$	0.241	5.69	11.14	85.12	0.242	5.67	11.12	85.12	0.241	5.67	11.08	85.04	−9.82	−2.85
$CuFeSe_2$	0.253	5.61	11.03	118.6	0.256	5.59	10.98	118.6	0.254	5.57	10.96	118.1	−5.31	7.48

[a]Shay and Wernick [29], [b]Medvedkin et al. [17], [c]Yu et al. [30].

To determine the stable state of all AMY_2 compounds at equilibrium, we calculated the spin-polarization total energy differences ΔE_1 ($\Delta E_1 = E_{FM} - E_{NM}$), representing the energy difference between NM and FM states, and ΔE_2 ($\Delta E_2 = E_{FM} - E_{AFM}$), representing the energy difference between AFM and FM states. The calculated ΔE_1 and ΔE_2 values for AMY_2 (A = Cu, Ag; M = Ti, V, Cr, Mn; Y = S, Se) are negative in Tables 1 and 2, indicating that the FM state is more favorable than the other two states in these compounds. Conversely, for $AFeY_2$, the calculated ΔE_2 values are positive, suggesting the stability of the AFM state in these compounds in Tables 1 and 2. Notably, from Tables 1 and 2, for $AScY_2$, the calculated ΔE_1 and ΔE_2 values are both zero, signifying the stability of these compounds in the NM state.

Our study demonstrates the significance of atomic and equilibrium lattice positions in influencing the magnetic and electronic properties of these solids. By conducting comprehensive calculations for these materials, the stable states of AMY_2 compounds at equilibrium were determined, providing valuable insights into their magnetic behavior.

The total energy for all AMY_2 compounds is fitted to Birch–Murnaghan's equation of state [25] in order to determine the equilibrium internal parameter u, tetragonal (c/a) ratio, lattice constants (a_0, c_0), and bulk modulus (B_0) for the NM, FM, and AFM states within GGA and LSDA. The calculated values are presented in Tables 1 and 2 under GGA. The bulk modulus (B_0) is also calculated to assess the mechanical stability using relation (1):

$$B_0 = -V_0 \frac{dp}{dv}. \tag{1}$$

From Tables 1 and 2, it can be observed that for small lattice parameters (a_0, c_0), the B_0 values are large, and vice versa. This change in lattice constants (a_0, c_0) and bulk modulus (B_0) is attributed to the effect of electronegativity between the Y [32] and M atoms, signifying that the atomic size of the M atom plays a crucial role in determining the ground state and magnetic properties of AMY_2 compounds. The estimated values of lattice parameters and bulk modulus agree with available experimental and theoretical results [17, 19].

Following geometry optimization, the relaxed cation–anion bond lengths R_{A-Y} and R_{M-Y} of (A = Cu, Ag; M = Ti, V, Cr, Mn, Fe; Y = S, Se) for the stable magnetic phase have been calculated under GGA and LSDA using relations (2) and (3) and presented in Table 3 for GGA scheme.

$$R_{A-Y} = a\left[u^2 + \frac{(1+\eta^2)}{16}\right]^{1/2}, \tag{2}$$

$$R_{M-Y} = a\left[\left(u - \frac{1}{2}\right)^2 + \frac{(1+\eta^2)}{16}\right]^{1/2}, \tag{3}$$

where R_{A-Y} and R_{M-Y} are the bond lengths of A—Y and M—Y, respectively. The bond lengths of A—Y and M—Y of AMY_2 either increase or decrease compared to the host $AGaY_2$ (A = Cu, Ag; Y = S, Se). The tetragonal ratio $\eta = c/2a$ is maintained at 1, preserving the local crystal structure of AMY_2 around the M atoms, which may either contract or expand for all the compounds without altering the chalcopyrite crystal symmetry. For AMY_2 (A = Cu, Ag; M = Ti, V, Cr, Mn; Y = S, Se) compounds, the calculated R_{M-Y} values are smaller than R_{A-Y} due to an increase in the electronegativity of Y atoms [32], attracting the M (Ti, V, Cr, Mn) atoms toward them when the value of $u > 0.280$. Conversely, R_{Fe-Y} is smaller than the bond lengths of R_{A-Y} due to the decrease in

Table 2: Calculated internal parameter (u), equilibrium lattice constants (a_0, c_0) in Å, and bulk modulus (B_0) in GPa, total energy difference ΔE_1 ($\Delta E_1 = E_{FM} - E_{NM}$) in meV/cell, ΔE_2 ($\Delta E_2 = E_{FM} - E_{AFM}$) in meV/cell between the nonmagnetic (NM), ferromagnetic (FM), and antiferromagnetic (AFM) states of $AgMY_2$ (M = Sc, Ti, V, Cr, Mn, Fe; Y = S, Se) using GGA.

Compounds	NM				FM				AFM				ΔE_1	ΔE_2
	u	a_0	c_0	B_0	u	a_0	c_0	B_0	u	a_0	c_0	B_0		
$AgGaS_2$	0.284	5.73	11.46	60.79	0.28	5.85	11.7	59	0.28	5.74	11.4	60.5	—	—
Others	0.284[a]	5.77[a]	11.54[a]	60.8[a]	—	—	—	—	—	—	—	—	—	—
Exp	0.282[b]	5.75[b]	11.50[b]	77.6[b]	—	—	—	—	—	—	—	—	—	—
$AgScS_2$	0.264	6.04	10.77	56.76	0.26	6.02	10.75	56	0.26	6.00	10.7	56.7	—	—
$AgTiS_2$	0.278	5.85	10.44	69.07	0.28	5.83	10.42	68	0.28	5.81	10.4	68.9	4.0	−6.0
$AgVS_2$	0.282	5.58	9.95	96.87	0.28	5.56	9.93	96	0.28	5.54	9.93	96.8	−5.4	−5.8
$AgCrS_2$	0.298	5.50	9.81	96.51	0.30	5.48	9.79	96	0.30	5.46	9.75	96.4	−9.5	−4.8
$AgMnS_2$	0.305	5.44	9.69	106.7	0.30	5.42	9.67	106	0.30	5.40	9.65	106	−7.66	−1.3
$AgFeS_2$	0.310	5.40	9.63	111.7	0.31	5.38	9.61	117	0.31	5.36	9.60	117	−7.61	4.5
$AgGaSe_2$	0.279	6.01	12.08	50.7	0.27	5.98	11.96	49	0.27	6.05	10.1	50.1	—	—
Others	0.279[a]	6.05[a]	12.08[a]	50.7[a]	—	—	—	—	—	—	—	—	—	—
Exp	0.272[b]	5.98[b]	11.96[b]	63.8[b]	—	—	—	—	—	—	—	—	—	—
$AgScSe_2$	0.252	6.12	11.16	49.08	0.25	6.10	11.12	49	0.25	6.08	11.1	49.0	—	—
$AgTiSe_2$	0.267	5.93	10.79	75.84	0.26	5.91	10.75	75	0.27	5.87	10.7	75.8	−6.7	−3.2
$AgVSe_2$	0.287	5.77	10.44	60.31	0.28	5.75	10.42	60	0.28	5.73	10.4	60.2	−6.2	−5.4
$AgCrSe_2$	0.297	5.64	10.20	71.64	0.29	5.62	10.18	71	0.29	5.60	10.1	71.6	−4.21	−6.34
$AgMnSe_2$	0.306	5.86	10.66	51.21	0.30	5.84	10.64	51	0.30	5.82	10.6	51.1	−7.5	−19.7
$AgFeSe_2$	0.309	5.68	10.28	98.32	0.31	5.66	10.26	98	0.31	5.64	10.2	98.2	−3.6	3.9

[a]Chen et al. [31], [b]Shay and Wernick [29].

Table 3: Calculated energy band gap (E_g) in eV, heat of formation (ΔH) in eV, and bond length in Å for the stable magnetic state of $CuMY_2$ and $AgMY_2$ (M = Sc, Ti, V, Cr, Mn, Fe; Y = S, Se) compounds using GGA.

Compounds (GGA)	FM			Compounds (GGA)	FM		
	ΔH	Bond length			ΔH	Bond length	
		Cu—Y	M—Y			Ag—Y	M—Y
$CuTiS_2$	−45.01	2.25	2.15	$AgTiS_2$	−34.29	2.55	2.34
$CuVS_2$	−68.39	2.27	2.18	$AgVS_2$	−36.13	2.56	2.26
$CuCrS_2$	−70.42	2.30	2.22	$AgCrS_2$	−34.36	2.57	2.19
$CuMnS_2$	−71.84	2.21	2.14	$AgMnS_2$	−44.51	2.58	2.16
$CuFeS_2$	−23.75 (AFM)	2.26 (AFM)	2.32 (AFM)	$AgFeS_2$	−43.41 (AFM)	2.57 (AFM)	2.56 (AFM)
$CuTiSe_2$	−39.31	2.42	2.38	$AgTiSe_2$	−55.52	2.46	2.36
$CuVSe_2$	−38.18	2.40	2.32	$AgVSe_2$	−51.25	2.23	2.18
$CuCrSe_2$	−38.77	2.37	2.28	$AgCrSe_2$	−27.66	2.21	2.10
$CuMnSe_2$	−39.44	2.29	2.13	$AgMnSe_2$	−54.41	2.16	2.05
$CuFeSe_2$	−40.10 (AFM)	2.26 (AFM)	2.35 (AFM)	$AgFeSe_2$	−32.08 (AFM)	2.11 (AFM)	2.15 (AFM)

the electro-positivity of the Fe atom in the $AFeY_2$ (A = Cu, Ag; Y = S, Se) compounds when the value of u is <0.280. The calculated R_{A-Y} and R_{Sc-Y} are equal in $AScY_2$ (A = Cu, Ag; Y = S, Se). Additionally, bond lengths are shorter in GGA compared to LSDA.

Furthermore, formation energies (ΔH) are calculated, providing information on the stability of AMY_2 (A = Cu, Ag; M = Ti, V, Cr, Mn, Fe; Y = S, Se) against decomposition into bulk constituents. These energies are calculated using expression (4):

$$\Delta H = \frac{1}{a+b+c}\left[E_{\text{Total}}^{\text{AMY}} - aE_{\text{Solid}}^{\text{A}} - bE_{\text{Solid}}^{\text{M}} - 2cE_{\text{Solid}}^{\text{Y}}\right]. \quad (4)$$

The calculated ΔH values of AMY_2 (A = Cu, Ag; M = Ti, V, Cr, Mn, Fe; X = S, Se) under GGA approximations are given in Table 3, respectively. The negative values of ΔH indicate that the AMY_2 compounds are thermodynamically stable with respect to lattice contraction, making it feasible to grow these compounds as thin films or multilayers on suitable semiconducting substrates.

The spin-dependent electronic band structures of stable magnetic AMY_2 (A = Cu, Ag; M = Ti, V, Cr, Mn, Fe; Y = S, Se) chalcopyrite's are calculated along the high symmetry directions in the first Brillouin zone to gain insight into the stabilization mechanism of the FM state. Since the results are

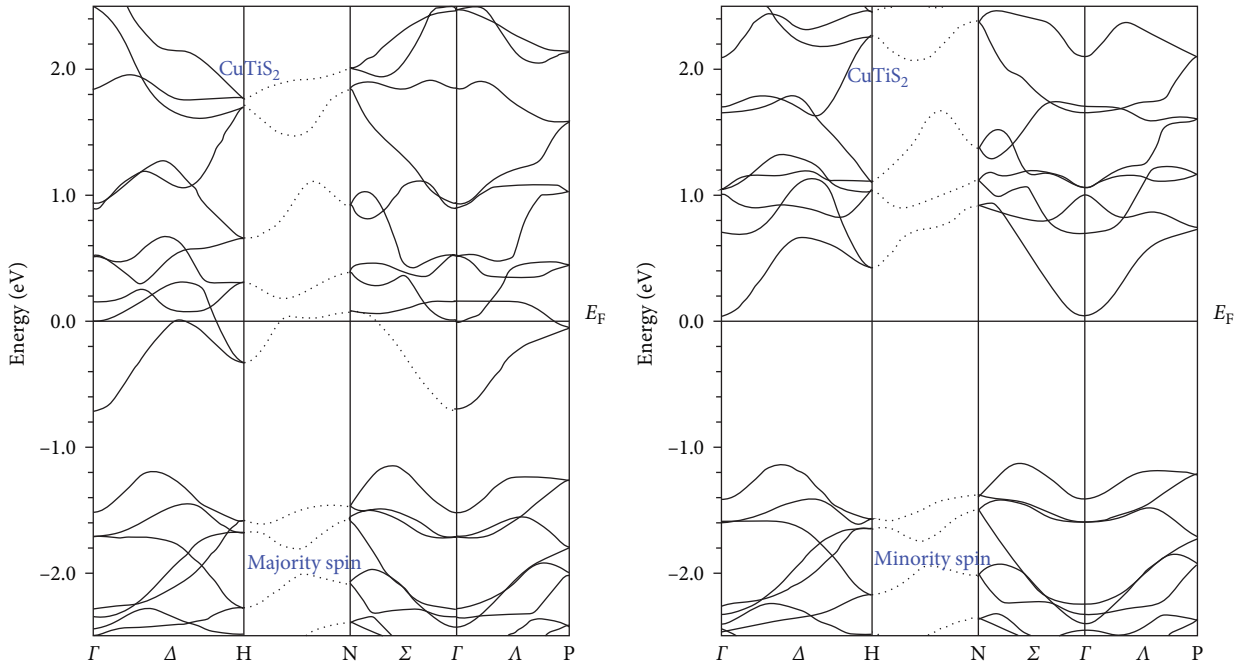

Figure 2: Spin-polarized electronic band structures of $CuTiS_2$ using GGA.

consistent under both GGA and LSDA schemes for AMY_2 (A = Cu, Ag; M = Sc, Ti, V, Cr, Mn, Fe; Y = S, Se), we depict the spin-polarized electronic band structures of $CuMS_2$ (M = Ti, Fe) compounds in Figure 2 for GGA. The substitution of M (Ti, Fe) atoms at the Ga site in $CuMS_2$ introduces −3d ("e_g" and "t_{2g}"))-like states of M atoms near the Fermi level (E_F) due to crystal field resonance. This results in the crystal field splitting of −3d ("e_g" and "t_{2g}") like states of M (M = Sc, Ti, Fe) atoms between the valence and conduction bands, converting direct band semiconductors into indirect bandgap semiconductors or metallic materials, as observed from the figures.

In Figure 2, the spin-polarized electronic band structure of $CuTiS_2$ demonstrates spin-splitting between the majority spin (spin-up) and minority spin (spin-down) states around the E_F. This spin-splitting of energy states is attributed to the hybridization of bonding e_g and antibonding t_{2g} suborbital of −3d states of Ti atoms with the nearest neighbor −3p states of S atoms, resulting in the formation of a broadband gap and behaving as a semiconductor in the spin-down channel. However, in the spin-up channel, these states cross the E_F and behave as metallic, indicating a half-metallic ferromagnet (HMF) property. Similar characteristics are observed in $CuTiSe_2$ and other electronic band structures of AMY_2 (A = Cu, Ag; M = V, Cr, Mn; Y = S, Se) compounds. These compounds likely possess an actual HMF property, and the calculated HM energy gaps (E_{HM}) and minimal energy gaps ($E_g\downarrow$) under GGA for AMY_2 (A = Cu, Ag; M = Ti, V, Cr, Mn; Y = S, Se) are presented in Table 4.

However, identical band structures are observed for both spin-up and spin-down states of $CuFeY_2$ (Y = S, Se) within both LSDA and GGA approximations, as shown in Figure 3. Therefore, $CuFeS_2$ is found to exhibit an AFM metallic nature in its ground state, which is in agreement with earlier experimental [33] and DFT results [34–36]. The same phenomenon is observed in $CuFeSe_2$ and $AgFeY_2$ compounds, where the spin states of Fe atoms are antiparallel (Fe↑, Fe↓) to each other, transforming $AFeY_2$ (A = Cu, Ag; Y = S, Se) into AFM. The total spontaneous magnetization vanishes due to the appearance of an induced spin density wave, making both spin-up and spin-down states antiparallel and similar.

To gain insight into the nature of the chemical bonds and charge transfer between the atoms A, M, and Y of AMY_2 (A = Cu, Ag; M = Ti, V, Cr, Mn, Fe; Y = S, Se), electron charge density plots along the (110) plane for both up-spin and down-spin states of $CuMS_2$ (M = Ti, Fe) are shown in Figures 4 and 5 within GGA. General observations from these figures reveal that the charge density contours are spherical, with most of the charges accumulating around S atoms due to the formation of Cu—S and M—S bonds and charge transfer of valence electrons from Cu to S and M to S in $CuMS_2$, indicating a mixture of ionic and covalent bonding between them.

For $CuTiS_2$, significant charge transfer between Ti and Y ions is observed due to the high degree of covalence between them, leading to the movement of the Ti ion toward S atoms in Figure 4. A similar bonding nature is present in $CuTiSe_2$ and $AgMY_2$ (M = V, Cr, Mn; Y = S, Se) compounds, with an increase in covalence and less ionic character. The central part of the atomic sites represents the core states, where the charge density varies rapidly. The red boundary around the contour signifies weak or partial bonding between the atoms A and Y and M and Y, while the white region indicates a lower electric charge.

Table 4: Calculated half-metallic gap (E_{HM}) in eV, minority spin gap ($E_g\downarrow$) in eV, partial, interstitial, and total and magnetic moments in μ_B for $CuMY_2$ and $AgMY_2$ (M = Sc, Ti, V, Cr, Mn, Fe; Y = S, Se) compounds at their equilibrium volume using GGA.

Compounds	GGA							Compounds	GGA						
	E_{HM}	$E_g\downarrow$	Magnetic moment						E_{HM}	$E_g\downarrow$	Magnetic moment				
			Cu	M	Y	Int	Total				Ag	M	Y	Int	Total
$CuTiS_2$	1.259	0.346	−0.018	0.735	−0.03	0.677	1.00	$AgTiS_2$	2.028	0.42	0.003	0.544	−0.008	0.54	1.00
$CuVS_2$	1.205	0.323	−0.042	1.692	−0.06	0.926	2.00	$AgVS_2$	2.020	0.12	−0.007	1.563	−0.027	0.95	2.00
$CuCrS_2$	1.325	0.551	−0.075	2.729	−0.1	1.057	3.00	$AgCrS_2$	1.548	0.45	0.015	2.456	−0.024	1.06	3.00
$CuMnS_2$	0.987	0.350	−0.076	3.584	−0.03	1.086	4.00	$AgMnS_2$	1.680	0.46	0.014	3.345	0.018	1.09	4.00
$CuFeS_2$	—	—	0.045	2.678	0.069	0.867	0	$AgFeS_2$	—	—	−0.320	1.356	−1.014	1.17	0
$CuTiSe_2$	1.088	0.017	−0.028	0.774	−0.04	0.66	1.00	$AgTiSe_2$	1.662	0.48	0.00	0.674	−0.020	0.71	1.00
$CuVSe_2$	0.934	0.713	−0.06	1.758	−0.07	0.941	2.00	$AgVSe_2$	1.696	0.24	−0.033	1.662	−0.051	0.72	2.00
$CuCrSe_2$	1.496 1.35[a]	0.667 0.65[a]	−0.103 −0.097[a]	2.833 2.903[a]	−0.11 −0.16[a]	0.978 0.853[a]	3.00 3.00[a]	$AgCrSe_2$	1.593	0.50	−0.04	2.649	−0.066	0.88	3.00
$CuMnSe_2$	1.224	0.533	−0.051	3.674	−0.05	1.070	4.00	$AgMnSe_2$	1.284	0.16	−0.019	3.437	−0.006	0.53	4.00
$CuFeSe_2$	—	—	−0.456	3.471	−0.39	−1.95	0	$AgFeSe_2$	—	—	−0.012	1.384	−1.93	−1.16	0

[a]Yu et al. [30].

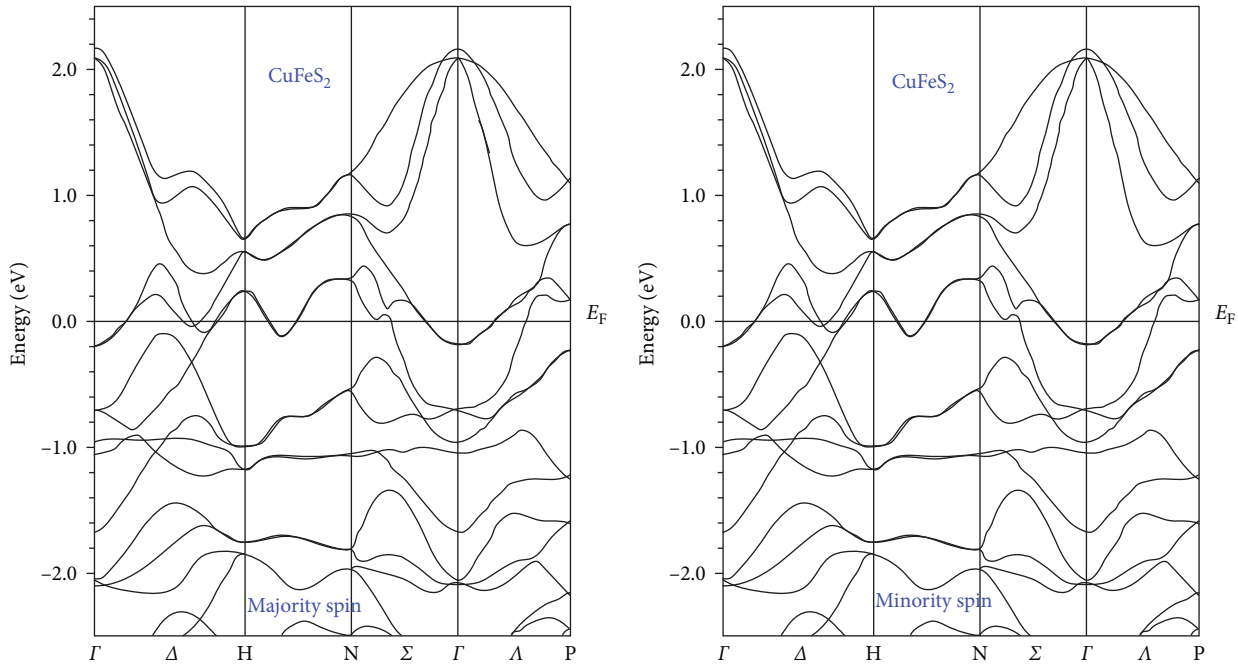

Figure 3: Spin-polarized electronic band structures of $CuFeS_2$ using GGA.

For $CuFeS_2$, the bond lengths R_{Cu-Fe} and R_{Fe-S} are almost the same in Figure 5. A similar chemical bond nature is observed in $CuFeSe_2$ and $AgFeY_2$.

To gain a deeper insight into the magnetic properties of AMY_2 (A = Cu, Ag; M = Ti, V, Cr, Mn, Fe; Y = S, Se) compounds, the total and partial density of states (PDOS) are calculated. Since the results are the same under LSDA and GGA for all AMY_2, we present the total and PDOS for GGA of $CuMS_2$ (M = Ti, Fe; Y = S, Se) in Figures 6 and 7. A general observation from the figures is that, in the valence region of $CuMS_2$, there is a combination of Cu (s), M (−3d (e_g and t_{2g})), and −3/4p of S/Se states, and they cross the E_F in the up-spin states. However, the behavior of valence electrons is different in the spin-down states.

The total and PDOS of $CuTiS_2$ in Figure 6 reveal a strong hybridization between the t_{2g} states of −3d Ti atoms and the nearest neighbor tetrahedral coordinated −3p states of S atoms, while the e_g states of Ti remain localized, exhibiting a nonbonding nature in the spin-down channel. The large exchange spin-splitting between the occupied e_g states and partially filled t_{2g} states of −3d Ti atoms and −3p states of S atoms, with a minor contribution from −s states of Cu atoms, pushes these states above the Fermi level in the minority spin. This indicates the presence of an indirect

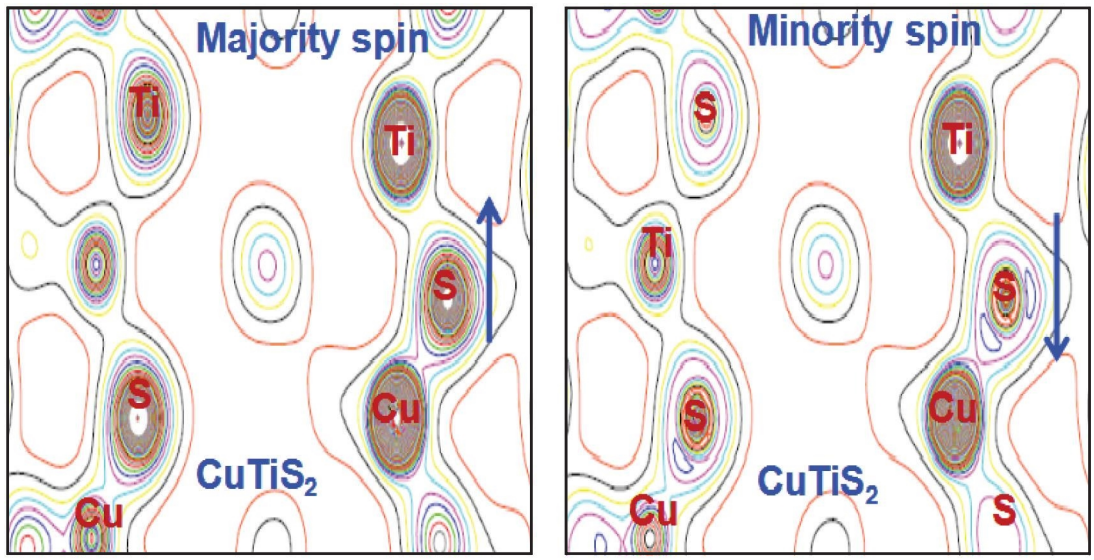

FIGURE 4: Valence electron charge density contours in the (110) plane for $CuTiS_2$ using GGA.

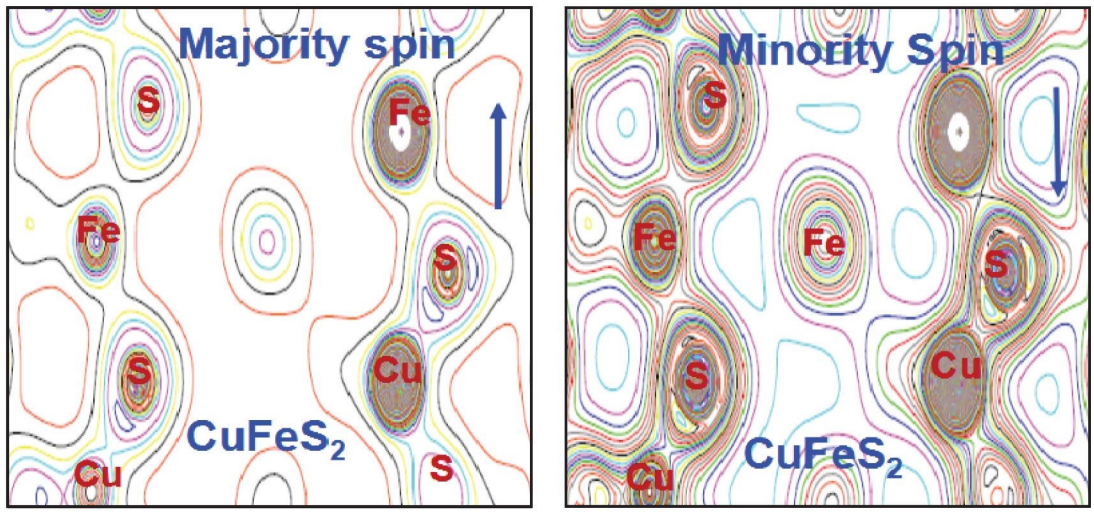

FIGURE 5: Valence electron charge density contours in the (110) plane for $CuFeS_2$ using GGA.

band gap between the valence band and conduction band in the spin-down channel. On the other hand, the t_{2g} states of the Ti atom are well hybridized with −3p-like states of S atoms, and these states are extended, crossing the Fermi level, resulting in a metallic nature in the spin-up channel, indicating the observation of HMF nature in the $CuTiS_2$ compound. Similar behavior is observed in $CuTiSe_2$ and $AgMY_2$ (M = V, Cr, Mn; Y = S, Se) compounds, preserving the HMF property in these compounds under both GGA and LSDA.

The DOS of $CuFeS_2$ in Figure 7 shows a small electron population near the Fermi level. Similar conducting properties are expected in both the spin-up and spin-down states, signifying that $CuFeS_2$ is AFM at equilibrium conditions. The hopping electrons in the conduction band are due to the hybridization of e_g and t_{2g} states of *d* states of Fe atoms with −3p states of S atoms, which reduces the kinetic energy between them when the magnetic ions (Fe) are antiparallel to each other. Similar observations are found in $CuFeSe_2$ and $AFeY_2$ (Y = S, Se) compounds.

The substitution of M (Sc, Ti, V, Cr, Mn, Fe) atoms at the Ga site of the hosts $AGaY_2$ (A = Cu, Ag; Y = S, Se) induces a net magnetic moment. Table 4 gives the calculated individual spin magnetic moments and total magnetic moment of AMY_2 under GGA. In $ATiY_2$ (A = Cu, Ag; Y = S, Se) compounds, the Ti ions share four of their valence electrons in bond formation, and the remaining one unpaired d electron is responsible for the total magnetic moment of 1.00 μ_B/f.u. In a similar way, other M (V, Cr, Mn) atoms share their valence electrons with the nearest neighboring S/Se atoms, and the remaining unpaired electrons are responsible for integer magnetic moments of 2.00, 3.00, and 4.00 μ_B per formula unit, respectively, for AMY_2 (A = Cu. Ag; M = V, Cr, Mn; Y = S, Se) compounds. In $AFeY_2$ (A = Cu, Ag; Y = S, Se), each S/Se atom interacts with the two A (s) and Fe (d) orbitals. The spins of

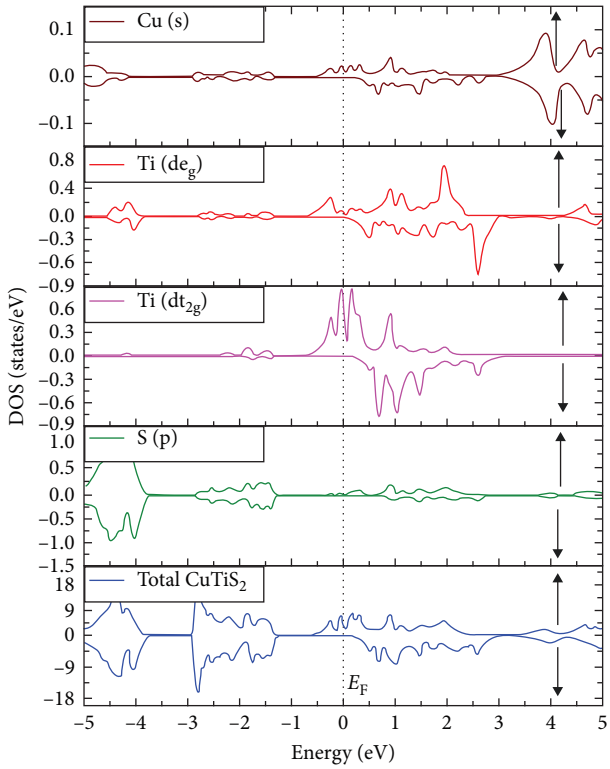

FIGURE 6: Spin-dependent total and partial density of states of $CuTiS_2$ using GGA.

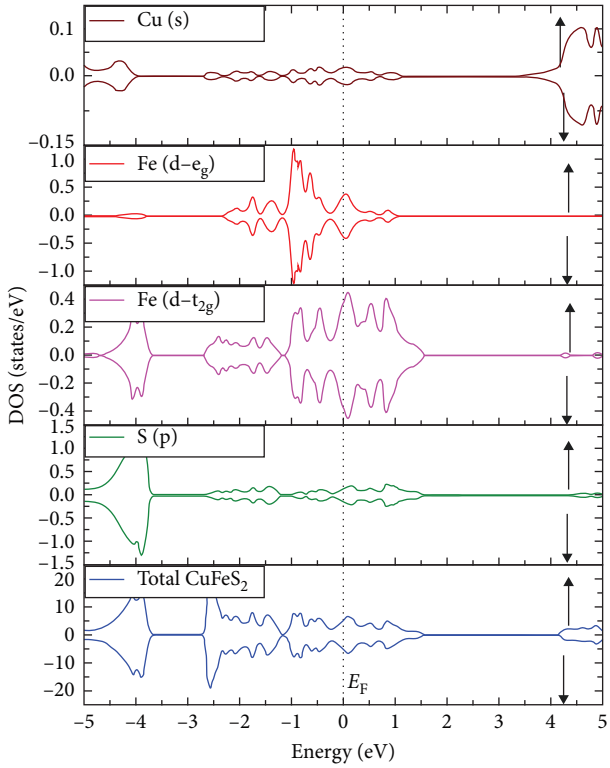

FIGURE 7: Spin-dependent total and partial density of states of $CuFeS_2$ using GGA.

the Fe atoms are aligned antiferromagnetically (Table 4). Due to this antiparallel spin arrangement, the net magnetic moments are zero, and the spin-up and spin-down channels are fully compensated by the local spin moments. The magnetic moment on each atomic site of $AScY_2$ (A = Cu, Ag; Y = S, Se) is zero, as there is no spin-polarization near the Fermi level. From Table 4, it is noticed that the magnetic moments are either small or negative for A and Y, indicating that they are antiparallel and localized primarily. The calculated net magnetic moment in AMY_2 (A = Cu, Ag; M = Ti, V, Cr, Mn, Y = S, Se) arises mainly from the M ions. The total magnetic moment of the tetrahedrally coordinated M atom is reduced due to the increase in the hybridization of M −3d (e_g and t_{2g}) states with the nearest-neighboring Y – (3p or 4p) states of S and Se from its space charge.

4. Conclusion

In conclusion, our study based on density functional calculations investigates the magnetic properties of AMY_2 (A = Cu, Ag; M = Sc, Ti, V, Cr, Mn, Fe; Y = S, Se) chalcopyrite's by substituting M ions at the Ga site of hosts $AGaY_2$ (A = Cu, Ag; Y = S, Se) using the FP-LAPW method within GGA and LSDA. We find that all the compounds are stable in the chalcopyrite structure, and the magnetic property appears in the nonmagnetic host upon the substitution of M atoms. Specifically, AMY_2 (A = Cu, Ag; M = Ti, V, Cr, Mn; Y = S, Se) exhibit ferromagnetic behavior, while $AFeY_2$ compounds show AFM characteristics at their equilibrium volume. On the other hand, the substitution of Sc does not induce ferromagnetism in $AScY_2$, indicating these compounds remain nonmagnetic. Moreover, the negative values of formation energy suggest that these compounds will be thermodynamically stable when synthesized experimentally.

Analyzing the electronic band structures and DOS, we find that the substitution of M atoms at the Ga site of $AGaY_2$ leads to stable HFM in AMY_2 (A = Cu, Ag; M = Ti, V, Cr, Mn; Y = S, Se) with the formation of an energy gap in the minority-spin channel. Meanwhile, the majority-spin channel exhibits strong metallic behavior, indicating the presence of HMF nature with 100% spin-polarization around the Fermi level. The origin of magnetism arises from the hybridization of −3d (t_{2g}) like states of M cations with the four nearest neighbor np-like states of Y (3p/4p) anions in the AMY_2 (A = Cu, Ag; M = Ti, V, Cr, Mn; Y = S, Se) compounds, resulting in integer magnetic moments of 1.00, 2.00, 3.00, and 4.00 μB per formula unit, respectively. For $AFeY_2$ compounds, AFM is achieved with the substitution of Fe atoms.

The HM gaps are found to be more stable with the lattice position at equilibrium, making it feasible to grow AMY_2 (A = Cu, Ag; M = Ti, V, Cr, Mn; Y = S, Se) compounds as thin films or multilayers on appropriate semiconducting substrates. The overall results demonstrate the potential of these materials for applications in spintronics and magnetic devices.

Data Availability

The data used to support the findings of this study are included within the article.

Conflicts of Interest

The authors declare no conflicts of interest.

References

[1] Y. Ohno, D. K. Young, B. Beschoten, F. Matsukura, H. Ohno, and D. D. Awschalom, "Electrical spin injection in a ferromagnetic semiconductor heterostructure," *Nature*, vol. 402, no. 6763, pp. 790–792, 1999.

[2] Y. Toual, S. Mouchou, A. Azouaoui et al., "First-principles calculations to investigate structural, electronic, magnetic, mechanical and thermodynamic properties of half-heusler alloy CoMnTe: using GGA and GGA+U methods," *Materials Chemistry and Physics*, vol. 307, Article ID 128115, 2023.

[3] Y. Toual, S. Mouchou, A. Azouaoui et al., "DFT+U investigations and Monte Carlo simulations on the structural, mechanical, electronic and magnetic properties of the half-heusler alloy CoMnSe for spintronics applications," *Physica B: Condensed Matter*, vol. 670, Article ID 415344, 2023.

[4] Y. Toual, S. Mouchou, U. Rani et al., "Probing electronic, magnetic and thermal properties of NiMnSb half-heusler alloy for spintronics as an environmentally friendly energy resource: a DFT+U and Monte Carlo study," *Materials Today Communications*, vol. 38, Article ID 108064, 2024.

[5] G. A. Medvedkin, K. Hirose, T. Ishibashi, T. Nishi, V. G. Voevodin, and K. Sato, "New magnetic materials in $ZnGeP_2$-Mn chalcopyrite system," *Journal of Crystal Growth*, vol. 236, no. 4, pp. 609–612, 2002.

[6] S. Cho, S. Choi, G.-B. Cha et al., "Room-temperature ferromagnetism in $(Zn_{1-x}Mn_x)GeP_2$ semiconductors." *Physical Review Letters*, vol. 88, no. 25 Pt 1, Article ID 257203, 2002.

[7] B. Kocak and Y. O. Ciftci, "Analysis of the structural, electronics and optic properties of Ni doped $MgSiP_2$ semiconductor chalcopyrites compound," *AIP Conference Proceedings*, vol. 1722, Article ID 220013, 2016.

[8] S. Cho, S. Choi, G. B. Cha et al., "Electronic and magnetic properties of $MnSnAs_2$," *Physica Status Solidi (B) Basic Research*, vol. 241, pp. 1462–1465, 2004.

[9] W.-H. Xie, Y.-Q. Xu, B.-G. Liu, and D. G. Pettifor, "Half-metallic ferromagnetism and structural stability of zincblende phases of the transition-metal chalcogenides," *Physical Review Letters*, vol. 91, no. 3, Article ID 037204, 2003.

[10] L. H. Yu, K. L. Yao, Z. L. Liu, and Y. S. Zhang, "Electronic structure and magnetic property of mnsn: prediction of half-metallic ferromagnetism in zinc-blende structure," *Solid State Communications*, vol. 144, no. 1-2, pp. 18–22, 2007.

[11] H. Akinaga, T. Manago, and M. Shirai, "Material design of half-metallic zinc-blende CrAs and the synthesis by molecular-beam epitaxy," *Japanese Journal of Applied Physics*, vol. 39, Article ID L1118, 2000.

[12] J. F. Bi, J. H. Zhao, J. J. Deng et al., "Room-temperature ferromagnetism in zinc-blende and deformed CrAs thin films," *Applied Physics Letters*, vol. 88, no. 14, Article ID 142509, 2006.

[13] W. Z. Wang, J. J. Deng, J. Lu, B. Q. Sun, X. G. Wu, and J. H. Zhao, "Structure, magnetization, and low-temperature spin dynamic behavior of zincblende Mn-rich Mn (Ga) as nanoclusters embedded in GaAs," *Journal of Applied Physics*, vol. 105, no. 5, Article ID 053912, 2009.

[14] S. C. Erwin and I. Žutić, "Tailoring ferromagnetic chalcopyrites," *Nature Materials*, vol. 3, no. 6, pp. 410–414, 2004.

[15] S. J. Pearton, Y. D. Park, C. R. Abernathy et al., "Ferromagnetism in GaN and SiC Doped with transition metals," *Thin Solid Films*, vol. 447, pp. 493–501, 1016, 2004.

[16] I. Žutić, J. Fabian, and S. D. Sarma, "Spintronics: fundamentals and applications," *Reviews of Modern Physics*, vol. 76, no. 2, pp. 323–410, 2004.

[17] G. A. Medvedkin, T. I. Takayuki Ishibashi, T. N. Takao Nishi, K. H. Koji Hayata, Y. H. Yoichi Hasegawa, and K. S. Katsuaki Sato, "Room temperature ferromagnetism in novel diluted magnetic semiconductor $Cd_{1-x}Mn_xGeP_2$, Japan," *Journal of Applied Physics*, vol. 39, no. 10A, Article ID L949, 2000.

[18] D. Vijayalakshmi, G. J. T. Ramachandran, G. Kalpana, and F. Hamed, "Unveiling the robust struct-electromagnetic characteristics of $CdAB_2$ Chalcopyrite (A = Cr, Mn, Fe; B = P, As): a comprehensive Ab-Initio study," *Advances in Condensed Matter Physics*, vol. 2023, Article ID 1754324, 13 pages.

[19] Y.-J. Zhao, P. Mahadevan, and A. Zunger, "Comparison of predicted ferromagnetic tendencies of Mn substituting the Ga site in III-V's and in I-III–VI2 chalcopyrite semiconductors," *Applied Physics Letters*, vol. 84, no. 19, pp. 3753–3755, 2004.

[20] J. P. Perdew and Y. Wang, "Accurate and simple analytic representation of the electron-gas correlation energy," *Physical Review B*, vol. 45, no. 23, pp. 13244–13249, 1992.

[21] J. P. Perdew, K. Burke, and M. Ernzerhof, "Generalized gradient approximation made simple," *Physical Review Letters*, vol. 77, no. 18, pp. 3865–3868, 1996.

[22] W. Kohn and L. J. Sham, "Self-consistent equations including exchange and correlation effects," *Physical Review*, vol. 140, no. 4A, pp. A1133–A1138, 1965.

[23] P. Blaha, K. Schwarz, F. Tran, R. Laskowski, G. K. H. Madsen, and L. D. Marks, "WIEN2k: an APW+lo program for calculating the properties of solids," *The Journal of Chemical Physics*, vol. 152, no. 7, Article ID 074101, 2020.

[24] F. Birch, "Finite elastic strain of cubic crystals," *Physical Review*, vol. 71, no. 11, pp. 809–824, 1947.

[25] J. C. Slater, "Wave functions in a periodic potential," *Physical Review*, vol. 51, no. 10, pp. 846–851, 1937.

[26] M. Dhilip, S. Rameshkumar, R. K. Raji et al., "Combined experimental and theoretical investigation on the structural, electronic, magnetic and optical properties of Pr_2CoFeO_6 double perovskite," *Materials Today Communications*, vol. 38, Article ID 108120, 2024.

[27] W. Fan, H. Yao, Y. Wang, and Q. Li, "Structural and optical characteristics of Sn-doped $CuGaSe_2$ thin films as a new intermediate band material for high-efficiency solar cells," *AIP Advances*, vol. 10, Article ID 065031, 2020.

[28] N. Sharma, M. Kouser, B. Chowhan, J. Kour, and M. Gupta, "Ag and Ce nanoparticles supported on silane-modified nitrogen-doped mesoporous carbon (Ag,Ce@SNC/A1SCA) obtained through green approach as heterogeneous catalyst towards the synthesis of 3,4-disubstituted isoxazol-5(4*H*)-one and polyhydroquinoline derivatives," *Materials Chemistry and Physics*, vol. 307, Article ID 128115, 2023.

[29] J. L. Shay and J. H. Wernick, *Ternary Chalcopyrite Semiconductors: Growth, Electronic Properties and applications*, Pergamon press, Oxford, 1975.

[30] B. Yu, W. Liu, S. Chen et al., "Thermoelectric properties of copper selenide with ordered selenium layer and disordered copper layer," *Nano Energy*, vol. 1, no. 3, pp. 472–478, 2012.

[31] S. Chen, X. G. Gong, and S.-H. Wei, "Band-structure anomalies of the chalcopyrite semiconductors $CuGaX_2$ versus $AgGaX_2$ ($X = S$ and Se) and their alloys," *Physical Review B*, vol. 75, no. 20, Article ID 205209, 2007.

[32] A. Janotti, S.-H. Wei, S. B. Zhang, and S. Kurtz, "Structural and electronic properties of $ZnGeAs_2$," *Physical Review B*, vol. 63, no. 19, 2001.

[33] C. Boekema, A. M. Krupski, M. Varasteh et al., "Cu and Fe valence states in $CuFeS_2$," *Journal of Magnetism and Magnetic Materials*, vol. 272-276, pp. 559–561, 2004.

[34] S. Conejeros, P. Alemany, M. Llunell, I. de P. R. Moreira, V. Sánchez, and J. Llanos, "Electronic structure and magnetic properties of $CuFeS_2$," *Inorganic Chemistry*, vol. 54, no. 10, pp. 4840–4849, 2015.

[35] M. A. Contreras, B. Egaas, K. Ramanathan et al., "Progress toward 20% efficiency in $Cu(In,Ga)Se_2$ polycrystalline thin-film solar cells," *Progress in Photovotaics*, vol. 7, no. 4, pp. 311–316, 1999.

[36] Y. Toual, S. Mouchou, A. Azouaoui et al., "DFT+U investigations and Monte Carlo simulations on the structural, mechanical, electronic and magnetic properties of the half-heusler alloy CoMnSe for spintronics applications," *Physica B*, vol. 670, Article ID 415344, 2023.